Strong Green Photoluminescence in Zr 3 N 4 Thin Films with an Orthorhombic Structure

Yuhe Liu, Nina Ge, Kunlun Wang, Niannian Li, Hui Sun, Jean-François Pierson, Bo Dai, Yong Wang

Strong Green Photoluminescence in Zr_3N_4 Thin Films with Orthorhombic Structure

Yuhe Liu[1], Nina Ge[2], Kunlun Wang[1], Niannian Li[1], Hui Sun[1], Jean-Francois Pierson[3], Bo Dai[2], Yong Wang[1,*]

AFFILIATIONS

[1] School of Space Science and Physics, Shandong University, Weihai 264209, China.

[2] State Key Laboratory for Environmental-friendly Energy Materials, Southwest University of Science and Technology, Mianyang 621010, China.

[3] Institut Jean Lamour, UMR 7198-CNRS, Université de Lorraine, Nancy F-54011, France.

[*]**Authors to whom correspondence should be addressed:** wang.yong06@sdu.edu.cn

ABSTRACT:

Green light causes the maximum luminous sensation in human eyes, which will bring many advantages for potential uses. However, the efficiency of light-emitting diodes (LEDs) in the green wavelength range (495-570 nm) is much lower than that in red or blue regions, which is known as the "green gap" problem. In this study, we report the strong green photoluminescence in metastable Zr_3N_4 thin films with orthorhombic structure for the first time. Crystallized Zr_3N_4 thin films have been successfully grown by high-power impulse magnetron sputtering. Notable green photoluminescence in the wavelength region of 490-535 nm has been identified in such orthorhombic Zr_3N_4 thin films even at room temperature. In addition, a joint experimental and theoretical study has been performed to investigate its electronic structures and to reveal the origins of such green light emissions. The calculations of the transition dipole moments demonstrate that the direct transition between the conduction band minimum and the energy level II below the valence band maximum are responsible for such strong green photoluminescence. This work may pave a new way to solve to the "green gap" problem in LEDs with low cost.

Keywords: Nitride semiconductors; Thin films; Green photoluminescence; Electronic structure;

1. INTRODUCTION

Metal nitrides are a special class of materials, which have been widely studied in both traditionally mechanical parts and modern electronic or optoelectronic devices.[1-4] For an example, rocksalt nitrides (such as TiN, ZrN and HfN) with superior hardness and corrosion resistance have been extensively applied as wear-resistance coatings.[5-8] The high conductivity and stability of TiN and TaN also facilitate them to be the diffusion barrier layers in integrated circuits.[9, 10] The second case is the III-nitride-based light-emitting diodes (LEDs), which have become the most promising candidates for high efficiency solid state lighting (SSL), since the first breakthrough of high-brightness InGaN-based LEDs in 1990s.[11, 12] Currently, the external quantum efficiency (EQE) of InGaN-based blue LEDs already exceed 80%.[13, 14] However, for the wavelengths beyond 490 nm, the EQE of these InGaN-based LEDs decreases significantly when the wavelength increases. Coincidentally, the phosphide-based LEDs of AlGaInP, exhibit a dramatical drop of EQE for wavelengths shorter than 570 nm.[15, 16] Thus, the commercialized LEDs in the wavelength region of 490 - 570 nm to match the high spectral sensitivity of the human visual perception of brightness are still absent, which is known as the "green gap" problem.[13, 17] Therefore, it is of great value to investigate novel semiconductors with green emissions.

Among the various nitrides, binary Zr-N system has attracted much attention, where most of the research focused on the stable phase of ZrN with exceptional mechanical properties as mentioned above. In addition to this stable phase with cubic structure, theoretical calculations also predict the existence of metastable Zr_3N_4 with four different structures:[18-20] (1) the orthorhombic phase (O-Zr_3N_4) with a space group of *Pnam*. (2) the cubic spinel phase (C-Zr_3N_4 (Spinel)) with a space group of *Fd3m*. (3) the defective phase (D-Zr_3N_4) formed by ordered Zr vacancies in simple cubic phase ZrN. (4) the cubic Th_3P_4-type phase (C-Zr_3N_4 (Th_3P_4)) with a space group of *I43d*. The stable ZrN exhibits the metallic conduction with the low resistivity, whereas, metastable phases of Zr_3N_4 are calculated to be semiconductors. So far, only the metastable phase of C-Zr_3N_4(Th_3P_4) has been successfully synthesized by extreme conditions, which exhibits the hardness as large as 30-37 GPa.[21, 22] However, due to

the difficulty to fabricate the metastable phase of O-Zr_3N_4, its functional properties and electronic structures are still unknown.

In this work, orthorhombic Zr_3N_4 thin films have been successfully deposited on glass and silicon (100) substrates by high-power impulse magnetron sputtering (HiPIMS). Strong green photoluminescence has been identified in such thin films even at room temperature for the first time. In addition, the electronic structure, optical and mechanical properties of orthorhombic Zr_3N_4 have been investigated.

2. EXPERIMENTAL SECTION

2.1. Experimental details. Metastable Zr_3N_4 thin films were deposited on glass and Si(100) substrates by HIPIMS in Ar-N_2 reactive mixture. It was shown that the phase structure and preferred orientation of thin films are independent of the nature of non-matched substrate (glass or silicon), as the native amorphous SiO_2 layer on single crystal Si (100) substrate was not removed. No intentional heating was applied to the substrate holder. A Zr target (99.9% purity) with rectangular shape (360 x 80 x 8 mm) was connected to a HIPIMS power supplier (Analoge und Digitale Leistungselektronik GmbH, GX 150/1000). The Ar and N_2 flow rate were fixed at 40 and 6 sccm, respectively. The total sputtering pressure was 0.9 Pa. The distance between target and substrate was 115 mm. The power supply worked on the constant power mode with the average power of 300 W, the frequency of 1000 Hz and the duty cycle of 2%. In addition, ZrN thin films with gold color were also deposited by HIPIMS for a comparison. For this purpose, the Ar and N_2 flow rate were fixed at 160 and 4 sccm, respectively, and the total sputtering pressure was 0.5 Pa. The power supply worked on the constant power mode with the average power of 1000 W, the frequency of 1000 Hz and the duty cycle of 5%.

Thin film thickness was measured by a surface profilometer (XP-1). The resistance was measured by a four-point probing system (RTS-8). X-ray diffraction (XRD, Rigaku Ultima IV) with Cu Kα radiation (λ = 0.15406 nm) in Bragg Brentano configuration was used to analyze the phase structures. X-ray photoelectron spectroscopy (XPS) analyses were performed in an ultrahigh vacuum (UHV)

experimental setup equipped with a photoemission analyzer and an Al Kα (1486.7 eV) x-ray source (Thermo Scientific Escalab 250Xi+). The Ar^+ ion etching was performed to clean the surface until there is no evolution in the C-1*s* XPS core level spectra. Scanning electron microscope (SEM, FEI Nova NanoSEM 450) and transmission electron microscope (TEM, JEOL ARM 200F) were used to study the surface morphology and microstructure of thin films, respectively. The optical absorption coefficient was determined by an ultraviolet-visible-near-infrared (UV-Vis-NIR) spectrophotometry (Lambda 1050). Photoluminescence (PL, FLS980) spectra were recorded at different temperatures (80 – 300 K) using a laser with the wavelength of 365 nm. The hardness of thin films was measured by a Nanoindenter (TTX-NHT2).

2.2. Theoretical calculations. The electronic structure calculations of O-Zr_3N_4 were performed by the projectoraugmented-wave (PAW) pseudopotentials, as implemented in Vienna *ab* initio Simulation Package (VASP) code. The plane-wave cut off was set to 400 eV. The HSE06 hybrid functional was used, which can accurately predict the electronic structures of nitride semiconductors.[23-25] The HF mixing constant α of 0.25 was employed.[26] The generalized gradient approximation (GGA) of the Perdew-Burke-Ernzerh (PBE)[27] functional was used to calculate sum of the squares of the transition dipole moments (P^2) for the analysis of the probability of optical transition between different energy levels.[28]

3. RESULTS AND DISCUSSIONS

3.1. Identifying the structure of O- Zr_3N_4 thin films. The XRD diffractogram of nitrogen-rich zirconium nitride thin film with the thickness of 156 nm is shown in **Figure 1a**, which exhibits a diffraction peak at 2θ of about 34.0°. Referring to the standard diffraction patterns of ZrN (PDF#35-0753) and O-Zr_3N_4 (PDF#51-0646) in **Figure 1a**, it is difficult to identify the phase structure of such nitrogen-rich zirconium nitride thin film. But the electron diffraction pattern of TEM provides additional and valuable information (Supplementary Tabe S1, the lattice constants calculated by electron diffraction pattern are consistent with the reported result[29, 30]). As seen in **Figure 1b**, the electron diffraction pattern can be well indexed by the O-Zr_3N_4, rather

than cubic phases of ZrN, C-Zr_3N_4 (Spinel), D-Zr_3N_4 and C-Zr_3N_4 (Th_3P_4). The high resolution TEM (HRTEM) image is shown in **Figure 1c**, where the crystal planes with a distance of 0.31 nm are determined as the O-Zr_3N_4 (310). These evidences demonstrate the successful growth of O-Zr_3N_4 thin films. The resistivity of O-Zr_3N_4 thin films at 300 K is as high as 76000 Ω cm, whereas the ZrN thin film possesses the resistivity of 1.1 x 10^{-3} Ω cm.

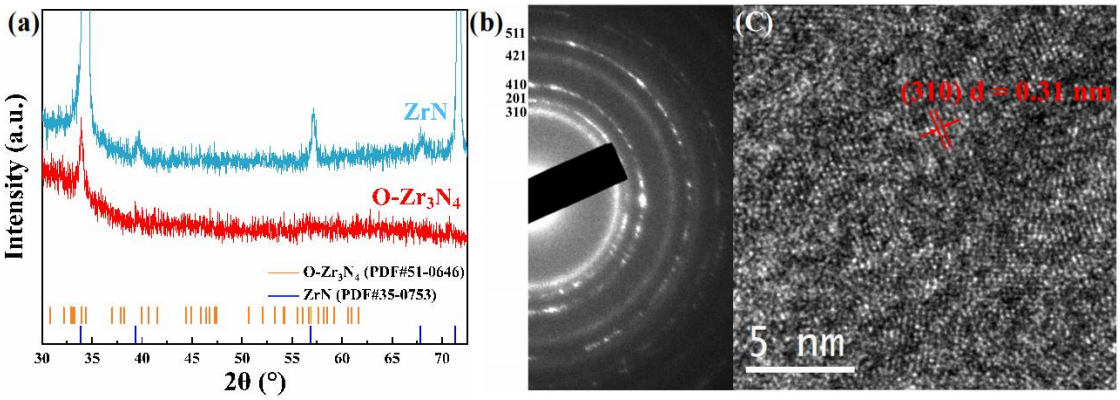

Figure 1. (a) The XRD diffractograms of ZrN and O-Zr_3N_4 thin films. The standard diffraction patterns of ZrN (PDF#35-0753) and O-Zr_3N_4 (PDF#51-0646) are also presented in the bottom. **(b)** The electron diffraction pattern and **(c)** the HRTEM image of O-Zr_3N_4 thin film.

The Zr-3*d* and N-1*s* core level XPS spectra of O-Zr_3N_4 are compared with those of ZrN (see **Figure 2**). As seen in **Figure 2a**, the Zr-3*d* peaks at the binding energy of 182 eV exhibit slight shift to higher energy, when changing the phases from ZrN to O-Zr_3N_4. On the contrary, the N-1*s* peaks move towards to lower binding energy, as shown in **Figure 2b**. These opposite directions of Zr-3*d* and N-1*s* are in agreement with the reported results,[30] where metallic ZrN was compared with insulator Zr_3N_4 with unknown phase structure. Such evolution tendency of binding energy is an indicator of electronic changes and charge transfer from Zr to N, which occurs when the phases change from ZrN to O-Zr_3N_4. Thus, the ionic bonding becomes stronger and the charge is more localized, giving rise to an insulator.[30]

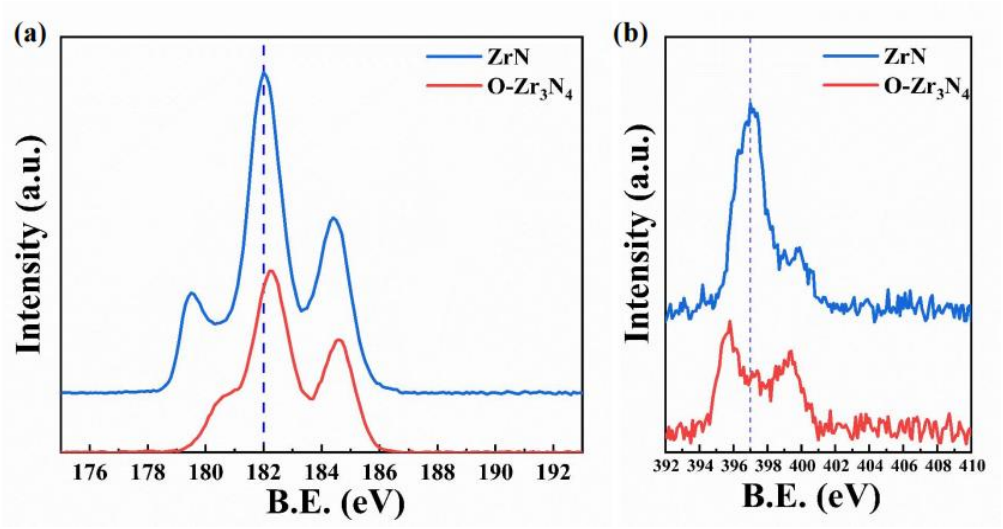

Figure 2. (a) Zr-3*d* and **(b)** N-1*s* core level XPS spectra of ZrN and O-Zr_3N_4 thin films.

3.2. Strong green photoluminescence identified in O-Zr_3N_4 thin film. The temperature-dependent photoluminescence (PL) properties of O-Zr_3N_4 thin film have been investigated from 80 to 300 K, as shown in **Figure 3**. Two luminescence peaks at about 2.4 and 1.97 eV are clearly evident in all PL spectra acquired at different temperature, as shown in **Figure 3a**. Especially, the luminescence peak of 2.4 eV located on the green wavelength range exhibit quite strong intensity, even at 300 K (see **Figure 3a**). It is worth noting that the both PL peaks do not shift with increasing temperature, which means that these light-emission are the intrinsic characters of O-Zr_3N_4, rather than from the defects. Meanwhile, the radiative lifetime of 1.6 μs obtained the time-resolved PL (see **Figure S1**) by is much larger than the PL lifetime of exciton emission in GaN and ZnO.[31, 32] Such luminescence peaks are asymmetrical broadening at high energy part, which is the characteristic of the PL spectra of indirect bandgap semiconductors.[33] We also investigate the power-dependent PL properties of O-Zr_3N_4 thin films (see **Figure 3b**). With the increase of laser power, the intensity of both peaks increases, while their positions do not shift. Specially, the peak intensities at 2.4 eV exhibit a linear relationship with the laser power. This also confirms that these light-emission are the intrinsic characters of O-Zr_3N_4.

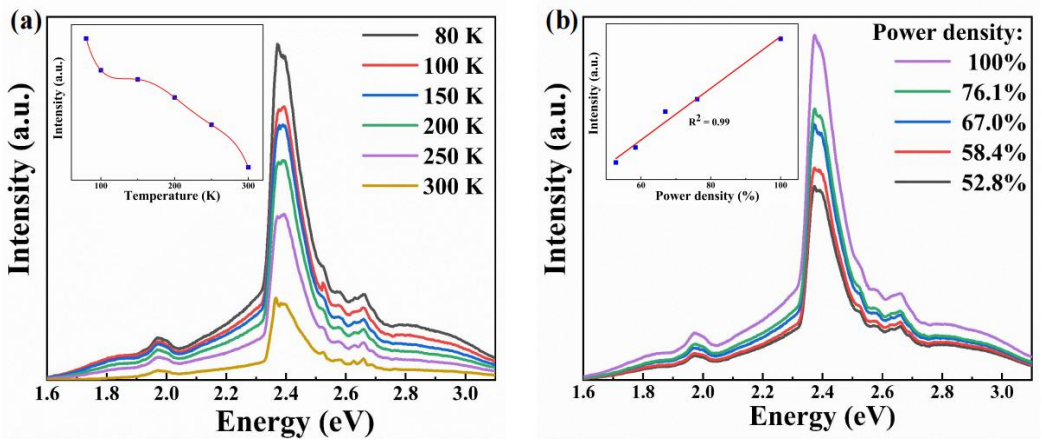

Figure 3. (a) Temperature-dependent and **(b)** power-dependent PL emission spectra of O-Zr_3N_4 deposited on glass substrate. The inset of (a) shows the relationship between the peak intensity at 2.4 eV and temperature, while the inset of (b) exhibits the linear relationship between the peak intensity at 2.4 eV and power density.

3.3. Electronic structures of O-Zr_3N_4. The electronic structures of O-Zr_3N_4 (Supplementary **Figure S2** for the crystal structure) have been calculated by first-principles calculations using the HSE06 functionals. The computed crystal constants (a =0.976 nm; b = 1.081 nm; c = 0.328 nm) are consistent with the experimental ones (a = 0.973 nm; b = 1.082 nm; c = 0.328 nm) achieved above. **Figure 4a** shows the electronic band dispersion of O-Zr_3N_4, demonstrating an indirect band gap of 1.72 eV. Such a value is much larger than the previous reported 0.68 eV calculated by GGA-PBE.[34] In addition, the experimental band gap of 1.8 eV is identified in O-Zr_3N_4 thin film by Tauc fitting of $(\alpha E)^{1/2}$ vs. E (α and E are the absorption coefficient and the photon energy, respectively), as shown in **Figure 4b**. This means the theoretical and experimental band gaps are well consistent.

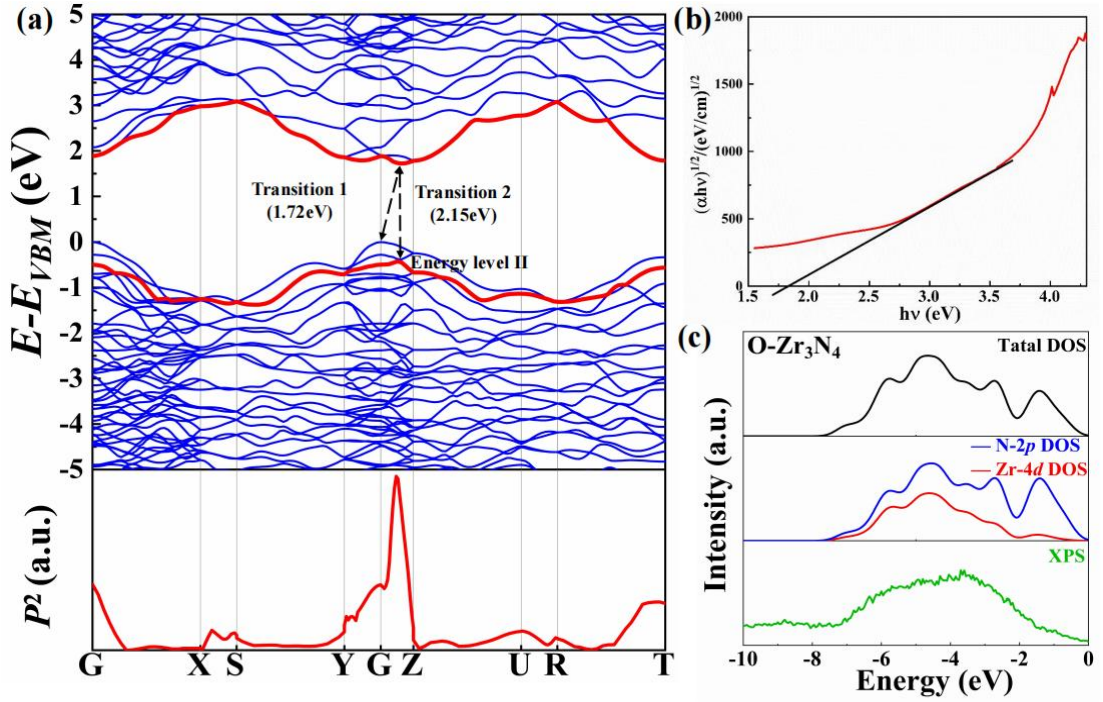

Figure 4. (a) Electronic band dispersion and corresponding P^2 of O-Zr_3N_4. (**b)** Tauc fitting of $(\alpha E)^{1/2}$ vs. E for O-Zr_3N_4 thin film. **(c)** Theoretically total DOS, Zr-4*d* and N-2*p* PDOS, are compared with the experimental photoemission valence band spectrum of O-Zr_3N_4.

The XPS valence band spectrum of O-Zr_3N_4 thin film is compared with the calculated density of states (DOS). Before discussing the results in detail, we briefly comment on the relative sensitivities of the Al Kα (1486.7 eV) photoemission source on the N-2*p* and Zr-4*d* spectral weights. The cross-section ratio of σ(N-2*p*) / σ(Zr-4*d*) $\approx$ 0.07 for Al Kα, is determined utilizing the known energy dependence of the photoionization cross-section.[35] This indicates that XPS primarily probes the Zr-*d* states. The XPS valence band spectrum and the DOS obtained from first-principles calculations of O-Zr_3N_4 are shown in **Figure 4c**, where the the valence band maximum (VBM) has been calibrated to 0 eV. The valence band structure of O-Zr_3N_4 can be divided into two main parts, as can be seen from the total DOS in **Figure 4c**. In the energy range of 0 to -1.8 eV, it is dominated by N-2*p* character. When the energy decreases to -1.9 to -6.7 eV, the contribution of Zr-4*d* gradually increases, and the electronic state is contributed from both Zr-4*d* and N-2*p*. Comparing Zr-4*d* partial density of states (PDOS) with XPS valence spectra, their spectral shape and peak

positions look quite close, as XPS primarily probes the Zr-*d* states as mentioned above.

As discussed above, the theoretically indirect bandgap of O-Zr_3N_4 is estimated to be about 1.72 eV (see **Figure 4a**). Thus, the peak at 1.97 eV in the PL spectra may be attributed to the indirect band gap transition between the conduction band maximum (CBM) and the valence band maximum (VBM), noted as transition 1 in **Figure 4a**. In order to investigate the origin of the notable green photoluminescence at about 2.4 eV in **Figure 4a**, the squares of the transition dipole moments (P^2) at various k points between several energy levels near the CBM and VBM were calculated (see Supplementary **Figure S3**), demonstrating that the direct transition between the CBM and the energy level II possesses the maximum transition probability (see **Figure 4a**). Looking at the energy band dispersion of O-Zr_3N_4 in **Figure 4a**, the direct transition between the CBM and the energy level II in the valence band exhibits a gap of 2.15 eV, which may correspond to the PL peak at 2.4 eV in **Figure 3a,** considering the slight dispersion between experiments and calculations. Therefore, it is believed that the direct transition between the CBM and the energy level II produces the strong green PL speak in O-Zr_3N_4. In addition, the potential epitaxial relationships between O-Zr_3N_4 and other nitride semiconductors to form heterojunction LEDs have also been investigated, which shows a mismatch of less than 1.5% of Zr_3N_4(001)||AlN(110) and Zr_3N_4(100)||GaN(010) (see Supplementary **Figure S4**). Therefore, it's believe that O-Zr_3N_4 may be able to fabricate high-efficiency green heterojunction LEDs.

3.4. Large hardness of O-Zr_3N_4 thin film. The hardness of O-Zr_3N_4 thin film has been measured by the Nanoindenter, yielding the hardness of 8.8 GPa (see Supplementary **Figure S5**). Such a value is even larger than traditional semiconductors in the forms of single crystal, such as Ge (111) (7.12 GPa), GaP (7.73 GPa), GaAs (6.8 GPa) and ZnO (4.7 GPa).[36] The hardness of O-Zr_3N_4 thin film is even close to that of GaN (0001) single crystal (10.2 GPa).[36] Such a large hardness of the O-Zr_3N_4 may be an additional benefit for its semiconductor applications.

4. CONCLUSIONS

In conclusion, the strong green photoluminescence in crystallized O-Zr_3N_4 thin films grown by high-power impulse magnetron sputtering was reported for the first time. Two emission peaks at approx.1.9 eV and 2.4 eV were observed in the photoluminescence spectra of O-Zr_3N_4 thin films, and these light-emissions are considered to be the intrinsic characters of O-Zr_3N_4. By combining experiments and first-principle calculations, the bandgap of O-Zr_3N_4 was determined to be about 1.8 eV, and the origins of two luminescence peaks were identified. Considering that O-Zr_3N_4 has the perfect lattice match with AlN and GaN (lattice mismatch less than 1.5%), O-Zr_3N_4 may be a promising candidate to fabricate the green LEDs with high efficiency.

SUPPORTING INFORMATION

See the supplementary materials for the additional crystal structure characteristics, electronic band dispersions, and the potential epitaxial relationships between O-Zr_3N_4 and other nitride semiconductors.

DATA AVAILABILITY

All data supporting the findings of this article and its Supplementary Information will be made available upon reasonable request to the authors. Source data are provided with this paper.

AUTHOR INFORMATION

Corresponding Authors

Yong Wang — School of Space Science and Physics, Shandong University, Weihai 264209, China; Email: wang.yong06@sdu.edu.cn

Authors

Yuhe Liu — School of Space Science and Physics, Shandong University, Weihai 264209, China

Nina Ge — State Key Laboratory for Environmental-friendly Energy Materials, Southwest University of Science and Technology, Mianyang 621010, China

Kunlun Wang — School of Space Science and Physics, Shandong University, Weihai 264209, China
Niannian Li — School of Space Science and Physics, Shandong University, Weihai 264209, China
Hui Sun — School of Space Science and Physics, Shandong University, Weihai 264209, China
Jean-Francois Pierson — Institut Jean Lamour, UMR 7198-CNRS, Université de Lorraine, Nancy F-54011, France
Bo Dai — State Key Laboratory for Environmental-friendly Energy Materials, Southwest University of Science and Technology, Mianyang 621010, China

Author contributions

Y.L. and Y.W. conceived the idea and designed the experiments. Y.L. carried out the growth, structural and optical characterizations, as well as the first-principle calculations. N.G. and B.D. contributed to first principle calculations and data analysis. K.W. participated the growth of thin film and performed the measurements of the hardness. N.L., Y.X., and H.S. performed the structural analysis. X.S. performed the TEM experiments and analysis. J.P. contributed the analysis and discussion for the results. Y.L. and Y.W. wrote the manuscript with the contributions from all the authors.

Notes

The authors declare no competing financial interests.

ACKNOWLEDGMENTS

Y.W. would like to acknowledge the Qilu Young Scholar at Shandong University, the Open Project of State Key Laboratory of Environment-friendly Energy Materials (21kfhg06), the Natural Science Foundation of Shandong Province (No. ZR2022MF261).

REFERENCES

1. Talley, K. R.; Perkins, C. L.; Diercks, D. R.; Brennecka, G. L.; Zakutayev, A. Synthesis of $LaWN_3$ nitride perovskite with polar symmetry. *Science* **2021,** *374* (6574), 1488-1491.
2. Lu, W. X.; Zhai, H.; Li, Q.; Chen, C. F. Pronounced Enhancement of Superconductivity in ZrN via Strain Engineering. *J. Phys. Chem. Lett.* **2021,** *12* (7), 1985-1990.
3. Lewin, E. Multi-component and high-entropy nitride coatings-A promising field in need of a novel approach. *J. Appl. Phys.* **2020,** *127* (16), 160901.
4. Zakutayev, A.; Bauers, S. R.; Lany, S. Experimental Synthesis of Theoretically Predicted Multivalent Ternary Nitride Materials. *Chem. Mater.* **2022,** *34* (4), 1418-1438.
5. PalDey, S.; Deevi, S. C. Single layer and multilayer wear resistant coatings of (Ti,Al)N: a review. *Mat. Sci. Eng. a-Struct.* **2003,** *342* (1-2), 58-79.
6. Staia, M. H.; Bhat, D. G.; Puchi-Cabrera, E. S.; Bost, J. Characterization of chemical vapor deposited HfN multilayer coatings on cemented carbide cutting tools. *Wear* **2006,** *261* (5-6), 540-548.
7. Purandare, Y. P.; Ehiasarian, A. P.; Hoveepian, P. E. Structure and properties of ZrN coatings deposited by high power impulse magnetron sputtering technology. *J. Vac. Sci. Technol. A* **2011,** *29* (1), 011004.
8. Diserens, M.; Patscheider, J.; Levy, F. Improving the properties of titanium nitride by incorporation of silicon. *Surf. Coat. Tech.* **1998,** *108* (1-3), 241-246.
9. Min, K. H.; Chun, K. C.; Kim, K. B. Comparative study of tantalum and tantalum nitrides (Ta_2N and TaN) as a diffusion barrier for Cu metallization. *J. Vac. Sci. Technol. B* **1996,** *14* (5), 3263-3269.
10. Ramanath, G.; Carlsson, J. R. A.; Greene, J. E.; Allen, L. H.; Hornback, V. C.; Allman, D. J. Gas-phase transport of WF_6 through annular nanopipes in TiN during chemical vapor deposition of W on TiN/Ti/SiO_2 structures for integrated circuit fabrication. *Appl. Phys. Lett.* **1996,** *69* (21), 3179-3181.
11. Zhu, D.; Wallis, D. J.; Humphreys, C. J. Prospects of III-nitride optoelectronics grown on Si. *Rep. Prog. Phys.* **2013,** *76* (10), 106501.
12. Nakamura, S.; Mukai, T.; Senoh, M. Candela-class high-brightness InGaN/AlGaN double-heterostructure blue-light-emitting diodes. *Appl. Phys. Lett.* **1994,** *64* (13), 1687-1689.
13. Maur, M. A. D.; Pecchia, A.; Penazzi, G.; Rodrigues, W.; Di Carlo, A. Efficiency drop in green InGaN/GaN light emitting diodes: the role of random alloy fluctuations. *Phys. Rev. Lett.* **2016,** *116* (2), 021401.
14. Narukawa, Y.; Ichikawa, M.; Sanga, D.; Sano, M.; Mukai, T. White light emitting diodes with super-high luminous efficacy. *J. Phys. D. Appl. Phys.* **2010,** *43* (35), 354002.
15. Mukai, T.; Yamada, M.; Nakamura, S. Characteristics of InGaN-based UV/blue/green/amber/red light-emitting diodes. *Jpn. J. Appl. Phys.* **1999,** *38* (7R), 3976-3981.
16. Krames, M. R.; Shchekin, O. B.; Mueller-Mach, R.; Mueller, G. O.; Zhou, L.; Harbers, G.; Craford, M. G. Status and future of high-power light-emitting diodes for solid-state lighting. *J. Disp. Technol.* **2007,** *3* (2), 160-175.
17. Jiang, Y.; Li, Y. F.; Li, Y. Q.; Deng, Z.; Lu, T. P.; Ma, Z. G.; Zuo, P.; Dai, L. G.; Wang, L.; Jia, H. Q.; Wang, W. X.; Zhou, J. M.; Liu, W. M.; Chen, H. Realization of high-luminous-efficiency InGaN light-emitting diodes in the "green gap" range. *Sci. Rep.-Uk* **2015,** *5*, 10883.
18. Ching, W. Y.; Xu, Y. N.; Ouyang, L. Electronic and dielectric properties of insulating Zr_3N_4. *Phys. Rev. B* **2002,** *66* (23), 235106.
19. Zerr, A.; Miehe, G.; Riedel, R. Synthesis of cubic zirconium and hafnium nitride having Th_3P_4 structure. *Nat. Mater.* **2003,** *2* (3), 185-189.

20. Saito, M.; Kura, C.; Toriumi, H.; Hinokuma, S.; Ina, T.; Habazaki, H.; Aoki, Y. Formation of mobile hydridic defects in zirconium nitride films with n-type semiconductor properties. *Acs Appl. Electron. Mater.* **2021,** *3* (9), 3980-3989.

21. Chhowalla, M.; Unalan, H. E. Thin films of hard cubic Zr_3N_4 stabilized by stress. *Nat. Mater.* **2005,** *4* (4), 317-22.

22. Taniguchi, T.; Dzivenko, D.; Riedel, R.; Chauyeau, T.; Zerr, A. Synthesis of cubic zirconium(IV) nitride, c-Zr_3N_4, in the 6-8 GPa pressure region. *Ceram. Int.* **2019,** *45* (16), 20028-20032.

23. Hinuma, Y.; Hatakeyama, T.; Kumagai, Y.; Burton, L. A.; Sato, H.; Muraba, Y.; Iimura, S.; Hiramatsu, H.; Tanaka, I.; Hosono, H.; Oba, F. Discovery of earth-abundant nitride semiconductors by computational screening and high-pressure synthesis. *Nat. Commun.* **2016,** *7*, 11962.

24. Kumagai, Y.; Harada, K.; Akamatsu, H.; Matsuzaki, K.; Oba, F. Carrier-induced band-gap variation and point defects in Zn_3N_2 from first principles. *Phys. Rev. Appl.* **2017,** *8* (1), 014015.

25. Chen, S. Y.; Narang, P.; Atwater, H. A.; Wang, L. W. Phase stability and defect physics of a ternary $ZnSnN_2$ semiconductor: first principles insights. *Adv. Mater.* **2014,** *26* (2), 311-315.

26. Perdew, J. P.; Ernzerhof, M.; Burke, K. Rationale for mixing exact exchange with density functional approximations. *J. Chem. Phys.* **1996,** *105* (22), 9982-9985.

27. Perdew, J. P.; Burke, K.; Ernzerhof, M. Generalized gradient approximation made simple. *Phys. Rev. Lett.* **1996,** *77* (18), 3865-3868.

28. Meng, W.; Wang, X.; Xiao, Z.; Wang, J.; Mitzi, D. B.; Yan, Y. J. T. j. o. p. c. l. Parity-forbidden transitions and their impact on the optical absorption properties of lead-free metal halide perovskites and double perovskites. *J. Phys. Chem. Lett.* **2017,** *8* (13), 2999-3007.

29. Ke, Y. E.; Chen, Y. I. Effects of Nitrogen Flow Ratio on Structures, Bonding Characteristics, and Mechanical Properties of $ZrN_{(x)}$ Films. *Coatings* **2020,** *10* (5), 476.

30. Prieto, P.; Galan, L.; Sanz, J. M. Electronic-structure of insulating zirconium nitride. *Phys. Rev. B* **1993,** *47* (3), 1613-1615.

31. Zhong, Y.; Wong, K. S.; Zhang, W.; Look, D. C. Radiative recombination and ultralong exciton photoluminescence lifetime in GaN freestanding film via two-photon excitation. *Appl. Phys. Lett.* **2006,** *89* (2), 022108.

32. Jen, F. Y.; Lu, Y. C.; Chen, C. Y.; Wang, H. C.; Yang, C. C.; Zhang, B. P.; Segawa, Y. Temperature-dependent exciton dynamics in a ZnO thin film. *Appl. Phys. Lett.* **2005,** *87* (25), 252117.

33. Cheng, T.-H.; Ko, C.-Y.; Chen, C.-Y.; Peng, K.-L.; Luo, G.-L.; Liu, C. W.; Tseng, H.-H. Competitiveness between direct and indirect radiative transitions of Ge. *Appl. Phys. Lett.* **2010,** *96* (9), 091105.

34. Yu, S. Y.; Zeng, Q. F.; Oganov, A. R.; Frapper, G.; Huang, B. W.; Niu, H. Y.; Zhang, L. T. First-principles study of Zr-N crystalline phases: phase stability, electronic and mechanical properties. *Rsc Adv.* **2017,** *7* (8), 4697-4703.

35. Yeh, J. J.; Lindau, I. Atomic subshell photoionization cross sections and asymmetry parameters: $1 \leqslant Z \leqslant 103$. *Atom. Data Nucl. Data* **1985,** *32* (1), 1-155.

36. Yonenaga, I. Hardness, yield strength, and dislocation velocity in elemental and compound semiconductors. *Mater. Trans.* **2005,** *46* (9), 1979-1985.

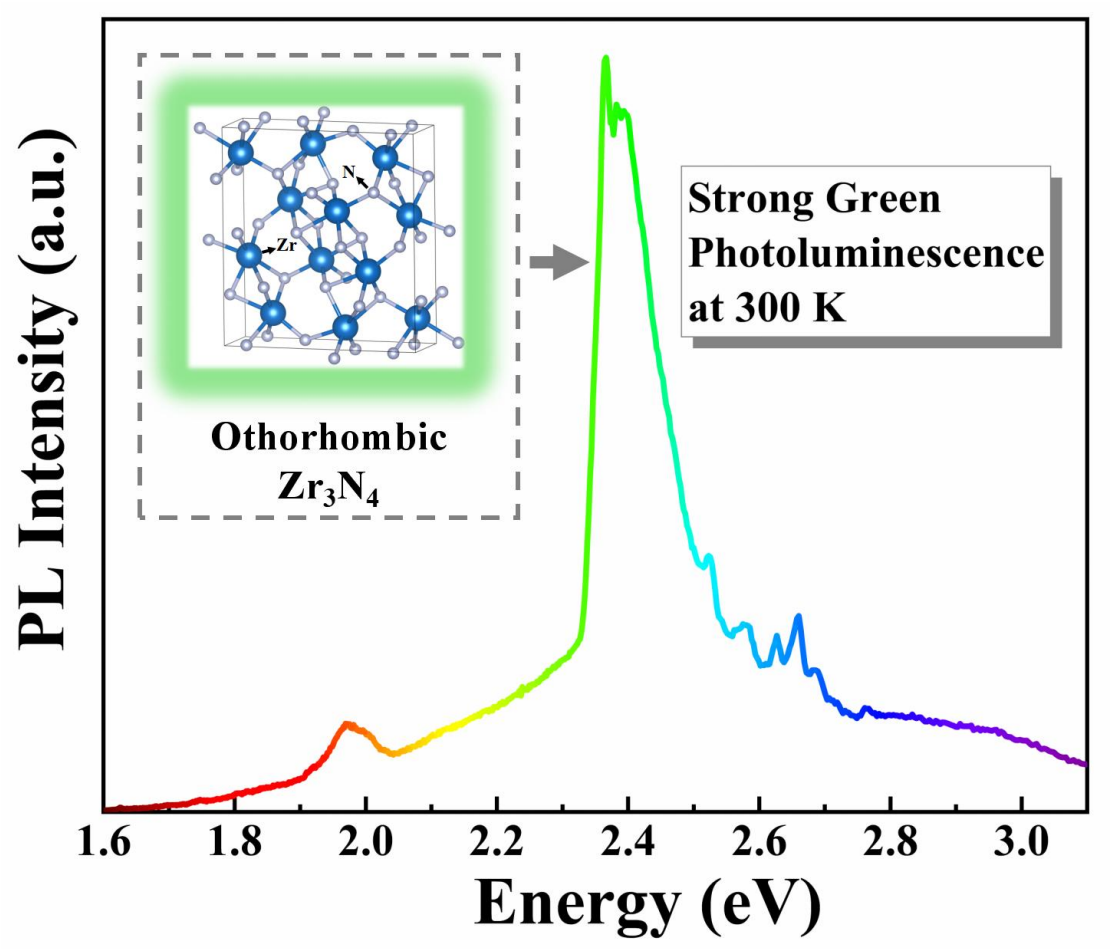
PL Intensity (a.u.)
Energy (eV)
1.6
1.8
2.0
2.2
2.4
2.6
2.8
3.0
N
Zr
Othorhombic
Zr3N4
Strong Green
Photoluminescence
at 300 K